# Learning Tree Interpretation from Object Representation for Deep Reinforcement Learning

**Anonymous Author(s)**
Affiliation
Address
email

## Abstract

Interpreting Deep Reinforcement Learning (DRL) models is important to enhance trust and comply with transparency regulations. Existing methods typically explain a DRL model by visualizing the importance of low-level *input features* with super-pixels, attentions, or saliency maps. Our approach provides an interpretation based on high-level *latent object features* derived from a disentangled representation. We propose a Represent And Mimic (RAMi) framework for training 1) an *identifiable* latent representation to capture the *independent* factors of variation for the objects and 2) a mimic tree that extracts the causal impact of the latent features on DRL action values. To jointly optimize both the fidelity and the simplicity of a mimic tree, we derive a novel Minimum Description Length (MDL) objective based on the Information Bottleneck (IB) principle. Based on this objective, we describe a Monte Carlo Regression Tree Search (MCRTS) algorithm that explores different splits to find the IB-optimal mimic tree. Experiments show that our mimic tree achieves strong approximation performance with significantly fewer nodes than baseline models. We demonstrate the interpretability of our mimic tree by showing latent traversals, decision rules, causal impacts, and human evaluation results.

## 1 Introduction

Deep neural networks have enabled Reinforcement Learning (RL) agents to extract relevant features from image observations and achieve human-level control by modeling action-value functions. Despite their promising performance, the learned knowledge remains implicit in these black-box neural structures, which hinders understanding the importance of input features and how they influence decisions. Previous DRL interpretations mainly aimed to visualize attention masks [1, 2] or saliency maps [3, 4] for input states. These interpretations are commonly based on entangled raw features in high-dimensional input space, and some recent studies [5, 6, 7] revealed that the generated attention masks are inconsistent for local samples in that very different attention distributions can yield equivalent predictions. Moreover, these point-wise importance maps do not identify the underlying causal relationships between target variables and complex inputs.

An alternative approach for generating post-hoc global explanations is mimic learning [8], which allows distilling the knowledge from an opaque DRL model to a transparent tree model. Some recent works [9, 10] built linear model trees to imitate the DRL action-value functions. These trees are learned for the high-dimensional input space; therefore they require numerous splits for building a tree with promising regression performance. The large tree size increases the complexity of their interpretations and makes it difficult to generate human-understandable decision rules. Previous models [11, 12] constrained the tree complexity by empirically setting some hyper-parameters (e.g, maximum depth), which, however, limits the mimic performance. It is unclear how to jointly optimize the simplicity and the fidelity of tree models to find a "sweet-spot".

Submitted to 35th Conference on Neural Information Processing Systems (NeurIPS 2021). Do not distribute.

To find an attractive trade-off between simplicity and fidelity, we develop a Represent And Mimic (RAMi) framework based on the Information Bottleneck (IB) principle [13]. The target of IB is learning a bottleneck representation to compress input signals while maximizing the information about a target variable, which defines *an information-theoretic objective* that views mimic learning as a data compression process. Our novel IB objective facilitates learning a *mimic tree* as the bottleneck to approximate the *action advantages* from the DRL model with a minimum number of splits. To learn IB-optimal mimic trees for DRL interpretation, RAMi integrates two major components.

1) An Identifiable Disentangling Object Encoder (IDOE) that detects objects from high-dimensional input space and learns an object representation to embed the objects with a limited number of latent variables. This representation is a) well-disentangled, meaning that each variable independently captures one factor of variation in a detected object, b) identifiable, allowing the mimic tree to uniquely extract the underlying causal relation from DRL models, and c) interpretable, in order to generate understandable DRL explanations. The interpretability is demonstrated with illustrative examples of latent traversals and human evaluation.

2) A Monte Carlo Regression Tree Search (MCRTS) algorithm that learns mimic trees based on the latent features from the object representation. MCRTS incorporates the IB principle into its search heuristic by deriving a Minimum Description Length (MDL) objective. Unlike previous tree learners that deterministically select a split by evaluating only its local influence, MCRTS looks ahead to global mimic performance and generates a compact distribution of candidate trees with explorations.

Our empirical evaluation shows that IDOE+MCRTS achieves a promising mimic performance with significantly fewer splits than other baseline models and an important reduction in the complexity of tree interpretation. To demonstrate how the learned mimic tree makes its target action-value function interpretable, we show causal relations and results of counterfactual interventions can be extracted from it. We study the validity of these interpretations by comparing with previous interpretable RL models and conducting a survey that collects human evaluations.

## 2 Related Works

We introduce previous works for interpreting DRL models.

**Self-Explainable Approaches:** Some recent works have explored self-explainable DRL models. To derive human-understandable policies, these models modified existing performance-driven DRL models (e.g., DQN) according to some specific designs, such as symbolic planning [14], decision trees [15, 16], Generalized Value Functions (GVFs) [17], Moore Machine Networks (MMNs) [18], transparent decision dynamics [19] or explainable feature extraction [1, 20]. These modifications influence the decision process of DRL agents for better interpretability.

**Post-hoc Interpretation:** An alternative approach is to generate posterior explanations for DRL models to achieve post-hoc interpretability. Existing methods commonly apply feature perturbation to generate saliency maps [3, 4] or learn attention masks [2, 21] with the attention neural network. These explanations are driven locally, based on computing a localization map that highlights the important regions for current actions. It is hard for these point-wise interpretations to maintain their consistency with explanations from other samples, which leads to unstable explanations [7]. Mimic learning (i.e., model distillation) [8] enables the generation of globally consistent explanations from a performance-driven DRL model. Previous works [10, 9] utilize mimic regression trees to interpret action values from DRL models, but their training objective did not control the model complexity and thus encouraged oversized mimic trees. Another recent work [22] proposed a tree regularizer that adjusts the loss function of deep models by integrating the regression performance of mimic trees. A recently proposed VIPER model [23] designed a Q-dagger algorithm to derive a tree-based policy function following online imitation learning [24]. Our experiments compare an updated VIPER model for predicting action advantages.

## 3 Represent and Mimic Framework

We propose a Represent And Mimic (RAMi) framework based on the Information Bottleneck (IB) principle. RAMi separately interprets the feature extraction and the decision making process of a DRL model with 1) an interpretable latent representation and 2) a transparent mimic tree.

### 3.1 Mimic Learning for DRL

RAMi follows the mimic learning [8] to learn post-hoc interpretations for a DRL model by transferring its knowledge to a mimic tree $\boldsymbol{\phi}$. To facilitate the knowledge distillation, mimic learners utilize soft-outputs from deep models as targets to supervise the training process of mimic trees. DRL models typically compute value functions ($V(\boldsymbol{s})$ or $Q(\boldsymbol{s}, \boldsymbol{a})$) to estimate the expected cumulative rewards at state $\boldsymbol{s}$. These value functions explicitly influence the RL decisions by controlling the policy gradient: $Q(\boldsymbol{s}, \boldsymbol{a})\nabla\pi(\boldsymbol{a}|\boldsymbol{s})$ [25] or determining the action: $\hat{\boldsymbol{a}} = \arg\max_{\boldsymbol{a}} Q(\boldsymbol{s}, \boldsymbol{a})$ [26]. Compared to the policy $\pi(\boldsymbol{a}|\boldsymbol{s})$, value functions reveal a more direct evaluation of the candidate actions or visited states. Based on the value functions, one can compute an advantage value for each action by subtracting a baseline: $y = Q(\boldsymbol{s}, \boldsymbol{a}) - V(\boldsymbol{s})$[1], which creates unbiased action-specific evaluations with less variance. Our mimic learner utilizes action advantages as the mimic targets, allowing us to understand when an action can outperform others by a certain advantage.

### 3.2 IB Method for Representing and Mimicking

We derive an objective for our RAMi framework based on the Information Bottleneck (IB) principle [13]. An ideal mimic tree achieves a promising approximation performance (fidelity) with a minimum number of splits (simplicity). The IB objective naturally integrates both goals, by encouraging a bottleneck representation to compress the input signals $X$ and preserve as much of the relevant information about mimic targets $Y$ (action advantages) as possible. The IB objective is:

$$\max_{\boldsymbol{\omega}} \Big[ I_{\boldsymbol{\omega}}(\Phi, Y) - \lambda I_{\boldsymbol{\omega}}(\Phi, X) \Big] \tag{1}$$

where $I$ denotes the mutual information, and $\lambda$ is a Lagrange multiplier. $-I_{\boldsymbol{\omega}}(\Phi, X)$ controls how much the mimic model compresses the input data, and $I_{\boldsymbol{\omega}}(\Phi, Y)$ measures how well the mimic model preserves information about targets[2]. The IB principle defines what we mean by a good representation, in terms of the fundamental trade-off between having a concise representation and one with good mimic performance [27]. However, in practice, it is difficult to learn a mimic tree from high-dimensional and entangled raw inputs (e.g., images and text embeddings), so we learn a latent object representation from input space and then build a mimic tree upon latent features. Inspired by the deep variational IB [27], The objective for our RAMi framework is:

**Theorem 1** *For a dataset with size N, let $1/N \sum_{n=1}^{N} \delta_{y_n}(y)\delta_{\boldsymbol{x}_n}(\boldsymbol{x})$ be the empirical data distribution that approximates $p(\boldsymbol{x}, y)$, let $\mathcal{L}_q(y_n) = -\log q(y_n|\boldsymbol{\phi})$ denote the description length for encoding the target $y_n$, let $\mathcal{L}_p(\boldsymbol{\phi}) = -\log p_0(\boldsymbol{\phi})$ denote the description length for encoding the mimic model $\boldsymbol{\phi}$. Optimizing the IB objective is equivalent to maximizing its lower bound, which is:*

$$\begin{aligned} &\frac{1}{N}\sum_{n=1}^{N} \Big\{ \mathbb{E}_{q(\boldsymbol{z}|\boldsymbol{x}_n)}[\log p(\boldsymbol{x}_n|\boldsymbol{z})] - \lambda \mathcal{D}_{KL}[q(\boldsymbol{z}|\boldsymbol{x}_n)\|p_0(\boldsymbol{z})] - \mathbb{E}_{q(\boldsymbol{z}|\boldsymbol{x}_n)} \Big[ \mathbb{E}_{q(\boldsymbol{\phi}|\boldsymbol{z})} \Big( \mathcal{L}_q(y_n) + \\ &\qquad \lambda \mathcal{L}_p(\boldsymbol{\phi}) \Big) - \lambda H[q(\boldsymbol{\phi}|\boldsymbol{z})] \Big] \Big\} \\ &= \textit{ELBo objective} + \textit{IB-MDL objective} + \textit{Entropy Regularizer} \end{aligned} \tag{2}$$

The *proof* can be found in appendix. This lower bound defines two sub-objectives: 1) the Evidence Lower Bound (ELBo) objective enables learning an object representation for inputs $q(Z|X)$ with our IDOE (Section 4). 2) The IB-MDL objective, with which we design a MCRTS algorithm (Section 5). MCRTS learns a compact distribution of mimic trees $q(\Phi|Z)$ where we select the optimal mimic tree $\boldsymbol{\phi}^*$ to achieve a "sweet-spot" between fidelity and simplicity.

## 4 Learning Object Representation

This section introduces the Identifiable Disentangling Object Encoder (IDOE) in our RAMi framework. The observed inputs from the RL environment are state-action-reward triplets $\boldsymbol{x}_n = [\boldsymbol{s}_n, \boldsymbol{a}_n, r_n]$, among which actions and rewards are often well-disentangled with limited dimensions, so our IDOE learns a disentangled latent representation for capturing the object features from states. We 1) introduce the key properties of IDOE that enable extraction of causal relationships, 2) describe the model structure and 3) discuss the interpretability for the learned latent representation.

[1] Action advantages can be defined as $V(\boldsymbol{s}') + r - V(\boldsymbol{s})$ if Q function is unknown (e.g., in A3C).

[2] $X$, $Y$, $Z$, and $\Phi$ are random variables; $\boldsymbol{x}$, $y$, $\boldsymbol{z}$, and $\boldsymbol{\phi}$ are instances of random variables, so $p(X)$ represents a distribution while $p(\boldsymbol{x})$ defines a probability. $F_{\boldsymbol{\omega}}(\cdot)$ is the functional parameterized by $\boldsymbol{\omega}$.

### 4.1 Disentangled Representation for Causal Interpretation

The high-dimensional state features from the RL environment are often *entangled* (e.g., highly correlated pixels in an image), which makes causal inference from the raw input space impossible. IDOE utilizes a Variational Auto-Encoder (VAE) framework [28] that converts state features to a disentangled latent representation (i.e., $p(Z) = \prod_{d=1}^{D} p(Z_d)$). By optimizing the latent representation toward the maximized generative performance for the observed states, the independent latent variables capture complete state information. It allows us to assume that there is *no* (unobserved or observed) confounder between two latent variables [29, 30]. This property enables mimic learners to model causal relations between latent variables $Z$ and the target variable $Y$ following a Causal Decision Tree [31]. (Section 6.2 shows examples of causal relations). Since the latent representation encodes complex RL states with only a few latent variables, the efficiency of causal inference is improved significantly. This improvement makes inference algorithms computationally tractable on image data.

### 4.2 Identifiability of Latent Representation

Identifiability is one of the most fundamental properties for uniquely identifying the causal relations between inputs and targets. If a latent representation is unidentifiable, there exists multiple distributions with the same generative performance, and the variables between two distributions can be completely *entangled*, meaning that they develop inconsistent factorizations for the same inputs [32] (e.g., check Section E.1 in appendix for the factorizations learnt by VAEs). Based on these distributions, the mimic learner can return many different causal relations between the latent and target variables, so the true causal relation cannot be uniquely identified.

To better understand this problem, we define the identifiability under the unsupervised representation learning setting: $p(Z)$ is identifiable up to $\sim_B$, if $\forall \boldsymbol{s} \in \mathcal{S}$, $p(\boldsymbol{s}) = \int p(\boldsymbol{s}|\boldsymbol{z})p(\boldsymbol{z})\mathrm{d}\boldsymbol{z} = \int p(\boldsymbol{s}|\boldsymbol{z}')p(\boldsymbol{z}')\mathrm{d}\boldsymbol{z} \implies \exists B, c$ s.t. $T(p(Z)) = BT(p(Z')) + \boldsymbol{c}$, where function $T$ computes sufficient statistics of a distribution, $\boldsymbol{c}$ is a vector, and $B$ is an invertible matrix (that represents a bijective mapping). If $B$ is a permutation matrix, we claim the identifiability is up to a permutation, otherwise up to scaling [33]. A previous work [32] proved that without including an inductive bias (e.g., specific model designs or additional observations), it is impossible to learn identifiable representations without supervising signals. To enforce identifiability of the latent object representation, IDOE 1) utilizes a Multi-Object Network (MONet) [34] structure that is specially designed to capture variations of objects, and 2) builds a conditionally factored prior $p(Z|A, R) = \prod_d p(Z_d|A, R)$ where each variable $Z_d$ has a univariate Gaussian distribution. Following an Identifiable VAE (IVAE) design [33], IDOE learns a conditional approximate posterior $q(Z|S, A, R)$ as the state representation.

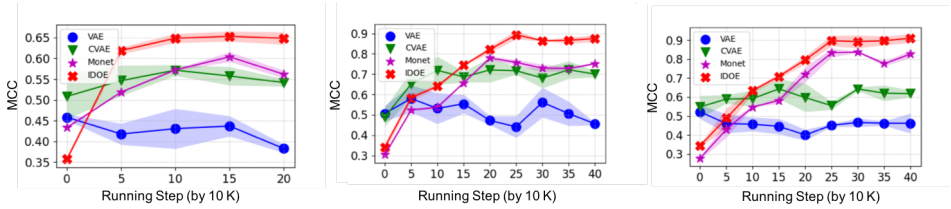


Figure 1: MCC scores for the examined variational encoders (including VAE, Conditional VAE, MONet and IDOE) trained in the Flappy Bird (left), Space Invaders (middle), and Assault (right) environments. We report the mean$\pm$variance MCC scores computed from three independent runs.

**Evaluation.** We evaluate the identifiability of IDOE by comparing its Mean Correlation Coefficient (MCC) with other variational encoders. MCC measures if we can identify latent variables from one model with variables from another model, up to point-wise transformations. To compute MCC, we 1) independently train two encoders based on the same structure, 2) average the correlation coefficients between paired latent variables from these encoders at different training steps, where pairing is done by solving a linear sum assignment problem to assign the latent variables from one encoder to another for the best overall correlation. The results (Figure 1) demonstrate that conditioning variables and an object network can consistently improve the identifiability of latent representations, whereas VAEs show no evidence of identifiability. This finding is consistent with [32, 33].

### 4.3 Model Implementation

IDOE decomposes a state $\boldsymbol{s}$ into object-level components with spatial masks $(m_1, ..., m_K)$ computed by a multi-layer convolutional attention network ($m_k$ indicates whether the $k^{th}$ object is present in

each pixel, see examples in Figure 2). Conditioning on $m_k$, $r$, and $\boldsymbol{a}$, IDOE independently encodes each component with an encoder-decoder Conditional VAE (CVAE). To train IDOE, we decompose the ELBo from our IB objective (Theorem 1) into an object-oriented variational lower bound:

$$\log \sum_{k=1}^{K} m_k p_d(\boldsymbol{s}|\boldsymbol{z}_k) - \beta \mathcal{D}_{KL}\Big(\prod_{k=1}^{K} q_{enc}(\boldsymbol{z}_k|\boldsymbol{s}, \boldsymbol{a}, r, m_k) \| p(\boldsymbol{z}|\boldsymbol{a}, r)\Big) - \sum_{k=1}^{K} \lambda \mathcal{D}_{KL}\Big(q(m_k|\boldsymbol{s}, \boldsymbol{a}, r) \| p_d(m_k|\boldsymbol{z}_k)\Big) \tag{3}$$

where 1) the *first* term is a decoder log-likelihood that defines the reconstruction performance for a mixtures of decoder outputs. The state decoder $p_d(\boldsymbol{s}|\boldsymbol{z}_k)$ is implemented by deconvolution layers. 2) The *second* term is the KL-divergence (KLD) between the conditional approximate posteriors for each component and a conditional prior. The approximate posterior is implemented by:

$$q_{enc}(\boldsymbol{z}|\boldsymbol{s}, \boldsymbol{a}, r, m_k) := \mathcal{N}(\boldsymbol{\mu}_q, diag(\boldsymbol{\sigma}_q^2)) \text{ s.t. } [\boldsymbol{\mu}_p, \boldsymbol{\sigma}_q^2] = \psi^q[\psi^{conv}(\boldsymbol{s}, m_k), \psi^{mlp}(\boldsymbol{a}, r)] \tag{4}$$

$\psi^{mlp}$ and $\psi^q$ are multi-layer perceptrons while $\psi^{conv}$ denotes a convolutional network. The prior $p(\boldsymbol{z}|\boldsymbol{a}, r)$ is implemented by another Gaussian function without $\psi^{conv}$. 3) The *last* term defines the KLD between the mask generated by the attention network and the mask reconstructed by the CVAE. Our attention network $q(m_k|\boldsymbol{s}, \boldsymbol{a}, r)$ is implemented by U-Net [35] and the mask decoder $p_d(m_k|\boldsymbol{z}_k)$ applies the same structure as our state decoder.

Learning an object representation for the RL states is applicable in practice since 1) a RL state can generally be represented by a limited number of objects, and 2) the agent can interact with the RL environment to generate sufficient data for learning such a representation. Object-Oriented RL [36, 37, 38] has demonstrated that an agent can master RL games by modeling the object dynamics, so we utilize features from the object representation as the inputs to mimic learners: we sample latent features $\boldsymbol{z}_k$ from each component posterior $q_{enc}(Z_k|S = \boldsymbol{s}, A = \boldsymbol{a}, R = r, M = m_k)$, concatenate them with the conditioning values, and feed the entire vector $[\boldsymbol{z}_{1,\dots,K}, \boldsymbol{a}, r]$ to MCRTS .

### 4.4 Interpreting Latent Variables

IDOE learns a symbolic abstraction of state space by representing object variations (e.g., shapes and locations) with latent variables. A latent variable $Z_{k,d}$ (the $d^{th}$ variable for the $k^{th}$ object) captures an independent factor of object variations. A common approach to reveal the information captured by $Z_{k,d}$ is latent traversing [34, 39, 40]: we randomly choose images and inspect how the reconstruction components change as $Z_{k,d}$ is traversed from (empirical) minimum to maximum values. Figure 2 illustrates the objects captured by attention masks from IDOE and shows two examples of latent traversals in a flappy bird environment. We include a human evaluation to demonstrate the interpretability of latent variables (Section 6.2).

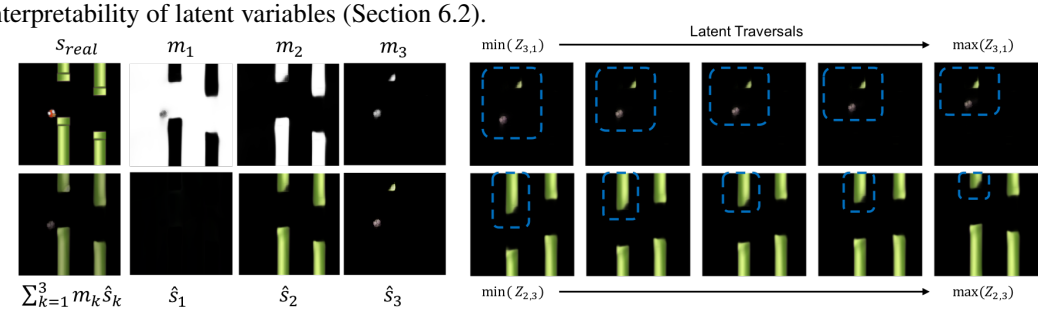


Figure 2: Visualizations for IDOE outputs. IDOE decomposes a state $\boldsymbol{s}_{real}$ into three objects with masks $m_1$ (for the background), $m_2$ (for pillars) and $m_3$ (for the bird), where *white/dark* colors mark *captured/uncaptured* regions. The generations from the decoder are $\hat{\boldsymbol{s}}_1$, $\hat{\boldsymbol{s}}_2$, and $\hat{\boldsymbol{s}}_3$. We show two latent traversals [41] for interpreting $Z_{3,1}$ (the $1^{st}$ variable for the $3^{rd}$ object) and $Z_{2,3}$ (the $3^{rd}$ variable for the $2^{nd}$ object). $Z_{3,1}$ captures the vertical distance between the bird and a pillar, and $Z_{2,3}$ captures the length of the left pillar (highlighted by blue frames).

## 5 Learning Mimic Tree Interpretations

This section introduces the approach to infer a mimic tree with the IB-MDL objective (in Theorem 1) and a Monte Carlo Regression Tree Search (MCRTS) algorithm to find the optimal tree.

### 5.1 Inferring Mimic Trees with IB-MDL

We define $\mathcal{L}_p(\phi)$ and $\mathcal{L}_q(y_n)$ in the IB-MDL objective for mimic tree inference. The goal of MDL is to find regularity and simplicity in the data by viewing learning as a compression problem. There are two agents with complete copies of the latent features $\boldsymbol{z}_n$, but only one agent knows the target

labels $y_n$. This agent must send the other agent a description of the missing labels using as few bits as possible, and we use a mimic tree to encode the information. The optimal mimic tree is defined to be the one that enables sending the minimum description length of (a) *encoding the tree structure* $\mathcal{L}_p(\phi)$, and (b) *encoding the exceptions* $\mathcal{L}_q(y_n)$ at each leaf node.

**(a)** *Encoding Tree Structure:* We convert the binary tree structure to a string that records the splits ($f$) and leaf predictions ($\hat{y}$) (e.g., 1,$f_0$,1,$f_1$, 0, $\hat{y}_0$, 0, $\hat{y}_1$, 0, $\hat{y}_2$ where we mark splits and leaves with 1 and 0) with depth-first search [42]. The encoding cost $\mathcal{L}_p(\phi)$ is:

**Proposition 1** *Given a regression tree with L splits, the total cost (in bits) of describing the tree structure with the string encoding method is:*

$$\mathcal{L}_p(\phi) = \log \frac{(2L-1)^2}{L^{\frac{3}{2}}(L-1)^{\frac{1}{2}}} + (2L-1)H(\frac{L}{2L-1}) + O(L^{-1}) \tag{5}$$

**(b)** *Encoding the Exceptions:* Traditional MDL tree algorithms [43] are proposed for classification trees to handle discrete labels. Their exception-encoding methods are infeasible with continuous predictions, so we utilize an alternative approach that models the distribution of action advantages at a leaf node $i$ with a Gaussian distribution $\mathcal{N}(\hat{y}_i^{tree}(\phi), \hat{\sigma}_i^2(\phi))$. Given a mimic tree $\phi$, $\hat{y}_i^{tree}$ and $\hat{\sigma}_i^2$ model the prediction and the scale of exception at the leaf $i$ respectively. Inspired by the variance reduction objective in classic regression trees, we utilize the log-variance to measure the cost of encoding exceptions, so $\mathbb{E}_{p(y_n)}[\mathcal{L}_q(y_n)] := \log\left[\sum_{i=0}^{L+1} \frac{N_i^{leaf}}{N}\hat{\sigma}_i^2\right]$ where $N$ and $N_i^{leaf}$ denote the total data size and the number of data points on the $i^{th}$ leaf node respectively.

### 5.2 MCRTS Implementation

MCRTS (Figure 3) takes latent features $\boldsymbol{z}_n \in \mathbb{R}^{K\times D}$ (K and D denote the number of objects and latent size respectively) from our IDOE and the conditioning values $\boldsymbol{a}_n, r_n$ as inputs. It explores different splits by maintaining multiple candidate mimic trees that are trained to approximate action advantages $Y$. To initiate a tree search, MCRTS stores all the instances (data points) in a cell $cell(\langle \boldsymbol{z}_1, \boldsymbol{a}_1, r_1; y_1\rangle, \langle \boldsymbol{z}_2, \boldsymbol{a}_2, r_2; y_2\rangle, \langle \boldsymbol{z}_3, \boldsymbol{a}_3, r_3; y_3\rangle, \dots)$ at the root node. An edge in the *MCRTS search tree* represents a split $f$ in the *mimic tree*. This binary split passes the instances from a parent cell to two partition cells in child nodes.

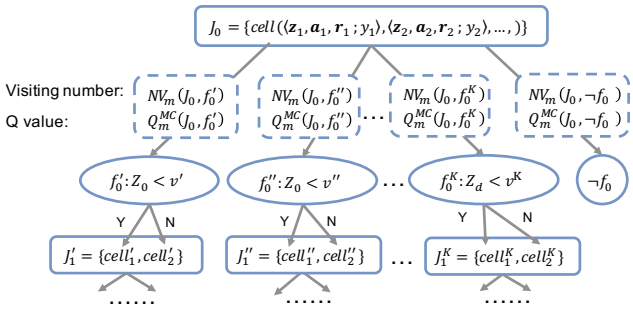


Figure 3: MCRTS structure, where a tree node records partition cells and an edge stores a number of visits $NV$ and an estimate $Q(J, f)$. $f_l^k : Z_d < v$ denotes the $k^{th}$ split at layer $l$, which checks whether $Z_d$ is smaller than a value $v$. The layer number $l$ equals the number of splits in a path. $\neg f_l$ denotes splitting ends.

Each MCRTS edge records a number of visits $NV(J, f)$ and an estimate $Q^{MC}(J, f)$ of the expected splitting influence. Each node $J$ contains a series of partition cells constructed by splits from the root node: $J := \{cell_1(\langle \boldsymbol{z}_1, \boldsymbol{a}_1, r_1; y_1\rangle, \langle \boldsymbol{z}_3, \boldsymbol{a}_3, r_3; y_3\rangle, \dots), cell_2(\langle \boldsymbol{z}_2, \boldsymbol{a}_2, r_2; y_2\rangle, \langle \boldsymbol{z}_4, \boldsymbol{a}_4, r_4; y_4\rangle, \dots), cell_3(\dots)\}$. MCRTS learns a compact distribution of mimic trees $p(\Phi|Z)$. *A mimic tree* $\phi \in \Phi$ *can be extracted from MCRTS by following a path from the root to a leaf node* $J_l$*, so* $\phi := \{f_0 \dots f_{l-1}, J_l\}$. A partition $cell_i$ in $J_l$ defines a leaf node in the mimic tree $\phi$, and the leaf prediction is $\hat{y}_i^{tree}$=$\sum_{y\in cell_i} y/N_i^{leaf}$. Appendix (E.1) provides a *mimic tree extraction* example.

**Searching:** MCRTS implements a tree search by running $M$ *plays* from a starting node $J_s$ (which is initialized to be the root node and updated after each *move*) with root parallelization [44]. At the $m^{th}$ play, MCRTS implements four phases including:

1) *Selection:* Traverse the tree from $J_s$ to a leaf node by selecting the split $f_{l,m}$ at each layer to maximize the Upper Confidence Bound (UCB) [45]:

$$f_{l,m} = \arg\max_f \left[Q_{m-1}^{MC}(J_l, f) + c_{puct}\frac{\sqrt{\log(m-1)}}{NV_{m-1}(J_l, f)+1}\right] \tag{6}$$

where $c_{puct}$ controls the scale of exploration. Similar to the entropy regularizer (Theorem 1), a large $c_{puct}$ prevents over-frequent visits to a node. *2) Evaluation:* Evaluate the selected leaf

Table 1: Mimic performance. We use the Variance Reduction (VR) and Variance Reduction Per Leaf (VR-PL) metrics since they are common regression objectives and optimized by the IB-MDL objective. Results for other regression metrics (Root Mean Square Error and Mean Absolute Error) and the corresponding variances are recorded in Table B.2 in appendix. $w_+$ indicates that each leaf node has an extra linear regression model.

| | Flappy Bird | | | Space Invaders | | | Assault | | |
|---|---|---|---|---|---|---|---|---|---|
| Method | VR | VR-PL | Leaf | VR | VR-PL | Leaf | VR | VR-PL | Leaf |
| Cart | 8.51E-2 | 8.43E-5 | 1007 | 4.96E-2 | 7.02E-5 | 705 | 4.79E-2 | 7.46E-5 | 642 |
| VIPER | 8.57E-2 | 1.88E-4 | 453 | 4.63E-2 | 8.80E-5 | 525 | 5.28E-2 | 8.09E-5 | 653 |
| M5-RT | **9.59E-2** | 8.37E-5 | 1144 | 4.54E-2 | 2.92E-5 | 1558 | 4.37E-2 | 2.73E-5 | 1605 |
| M5-MT | 9.56E-2 | 1.55E-4 | $612^{w_+}$ | 1.60E-2 | 1.23E-5 | $1303^{w_+}$ | 3.42E-2 | 2.54E-5 | $1351^{w_+}$ |
| GM-LMT | 8.99E-2 | 2.99E-4 | $303^{w_+}$ | 2.07E-2 | 8.32E-5 | $249^{w_+}$ | 5.55E-2 | 1.83E-4 | $307^{w_+}$ |
| VR-LMT | 8.46E-2 | 5.36E-4 | $157^{w_+}$ | 2.65E-2 | 1.61E-4 | $166^{w_+}$ | 5.80E-2 | 1.98E-4 | $291^{w_+}$ |
| VAE+CART | 7.25E-2 | 3.44E-4 | 212 | 3.99E-2 | 7.86E-5 | 507 | 5.15E-2 | 1.16E-4 | 448 |
| VAE+VIPER | 7.63E-2 | 5.32E-4 | 143 | 4.12E-2 | 9.89E-5 | 417 | 4.57E-2 | 1.29E-4 | 356 |
| VAE+GM-LMT | 6.35E-2 | 3.51E-4 | $180^{w_+}$ | 3.39E-2 | 2.75E-4 | $123^{w_+}$ | 4.20E-2 | 1.44E-5 | $293^{w_+}$ |
| VAE+VR-LMT | 7.95E-2 | 5.12E-4 | $154^{w_+}$ | 3.52E-2 | 2.08E-4 | $171^{w_+}$ | 5.10E-2 | 1.99E-4 | $258^{w_+}$ |
| VAE+MCRTS | 7.83E-2 | 1.27E-3 | 61 | 4.82E-2 | 5.66E-4 | 85 | 6.58E-2 | 7.75E-4 | 85 |
| IDOE+CART | 8.23E-2 | 4.02E-4 | 204 | 5.21E-2 | 1.38E-4 | 375 | 5.67E-2 | 1.81E-4 | 315 |
| IDOE+VIPER | 8.50E-2 | 4.48E-4 | 191 | 5.26E-2 | 1.69E-4 | 313 | 6.05E-2 | 1.90E-4 | 319 |
| IDOE+GM-LMT | 7.87E-2 | 3.74E-4 | $212^{w_+}$ | 4.79E-2 | 3.23E-4 | $149^{w_+}$ | 5.45E-2 | 2.15E-4 | $256^{w_+}$ |
| IDOE+VR-LMT | 8.21E-2 | 7.16E-4 | $115^{w_+}$ | 4.54E-2 | 3.79E-4 | $120^{w_+}$ | 6.03E-2 | 2.27E-4 | $268^{w_+}$ |
| IDOE+MCRTS | 8.53E-2 | **1.37E-3** | **62** | **5.37E-2** | **7.08E-4** | **76** | **7.53E-2** | **9.07E-4** | **83** |

$J_{leaf}$ with reward: $r^{MC}(J_{leaf}) = -\mathcal{L}_q(y_n) - \lambda\mathcal{L}_p(\phi)$. *3) Expansion:* Expand the leaf node with $G$ (the maximum exploration width) child nodes. *4) Back Up:* Update the action-values: $Q^{MC}_m = (Q^{MC}_{m-1}NV_{m-1} + r^{MC})/(NV_{m-1}+1)$ and increment the visit count: $NV_m = NV_{m-1}+1$ on all the traversed edges.

**Move:** After $M$ plays, we *move* $J_s$ to a child node by selecting the split $\tilde{f}_s = \arg\max_{f_k \in F_{1\ldots g(m)}} NV_m(J_s, f_k)$ and setting $J_s$ to a child node $\tilde{J}_{s+1}$ (connected by the edge $\tilde{f}_s$). The next play will start from the new starting node $\tilde{J}_{s+1}$. It allows MCRTS to prune the sub-optimal nodes [46].

# 6 Empirical Evaluation

We evaluate the mimic performance and demonstrate the interpretability of the mimic tree.

**Environment and Running Settings:** The evaluation environments include Flappy Bird, Space Invaders, and Assaults. Flappy Bird is a procedural game programmed with the pygame package [47]. The game states are randomly generated at each episode. Space Invaders and Assaults are commonly studied video games from OpenAI Gym toolkit [48]. (Check *data generation details* in Appendix).

**Baseline Models:** We compare previous tree-based mimic learners. The first baseline model is a Classification and Regression Tree (**CART** ) [49]. We include **VIPER** [23] as our second baseline by replacing its policy (decision) tree with a regression tree that imitates action values with a Q-dagger algorithm. The third baseline is the M5 [50] regression tree training algorithm. M5 constructs a piecewise constant tree by pruning the sub-optimal nodes. We include M5 with the Regression-Tree option (**M5-RT**) and the Model-Tree option (**M5-MT**). M5-MT builds a linear regression model for the instances at each leaf node while M5-RT maintains only a constant value. The last baseline is a Linear Model Tree (LMT) [9] for interpreting action values. A recent work [10] explored different heuristics for selecting splitting features, including Variance Reduction (**VR-LMT**) and Gaussian Mixture clustering (**GM-LMT**). The aforementioned models are directly learnt from raw input space (states and actions) [11]. To study the influence of latent representations, we evaluate their regression performance based on the latent features from both VAE and IDOE (Check appendix for the implementation details of baseline models).

## 6.1 Fidelity versus Simplicity

This experiment evaluates mimic trees by their 1) fidelity: how well a mimic model approximates the DRL model [9] and 2) simplicity: the size of these nonparametric trees. We divide the dataset (50k) into training (80%), validation (10%), and testing (10%) sets and generate 5 independent runs. Fidelity and simplicity are evaluated by the mimic performance and the number of leaves respectively.

Table 1 shows the regression performance. MCRTS+IDOE achieves a promising regression performance with significantly fewer leaves than other baseline models. This is because 1) IDOE learns a concise object representation from RL states and this representation outperforms that modelled by an unidentifiable VAE. 2) MCRTS selects splits to maximize the regression performance at a global

level, yielding a mimic tree with better fidelity. Apart from these obvious advantages, we find that some latent features may be indistinguishable for predicting action values, and this explains why some trees have better regression performance by building a large tree from raw inputs, but the large tree size compromises their interpretability.

**Leaf-by-Leaf Regression Performance:** To study the regression efficiency, we evaluate the per-leaf regression performance of examined models based on the latent features from IDOE. Figure 4 illustrates the performance of examined mimic trees when we constrain their number of leaves. MCRTS achieves a leading regression performance, as it selects a split by looking ahead to the future cumulative rewards instead of its local influence. Another key observation is that a well-explored split from MCRTS can beat a greedy split with extra linear regressors at leaf nodes (e.g., LMTs), allowing MCRTS to substantially improve the learning efficiency.

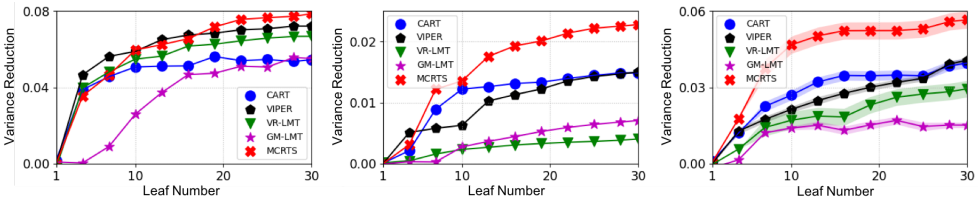


Figure 4: Leaf-by-leaf tree regression results based on latent features from IDOE in the Flappy Bird (left), Space Invaders (middle), and Assault (right) environments.

## 6.2 Illustrative Examples of Interpretable Mimic Trees

We demonstrate the interpretability of our mimic tree by 1) illustrating the extracted rules and causal relations, 2) comparing with previous RL interpretations and 3) conducting human evaluations. For clarity, this section uses the Flappy Bird environment as an example, where a DRL agent earns rewards by controlling a bird to pass pillars.

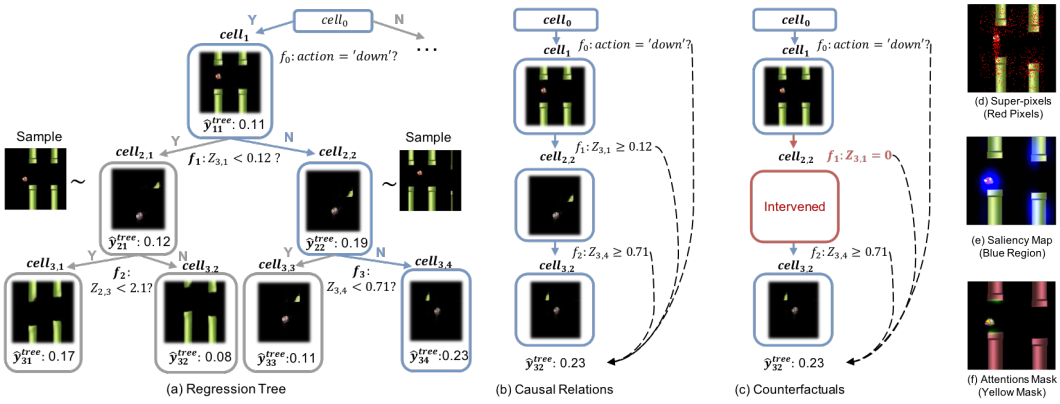


Figure 5: Mimic tree. $f_l : Z_{k,d} < v$ indicates the $l^{th}$ tree split is at $Z_{k,d}$ ($d^{th}$ variable for the $k^{th}$ object) with a splitting value $v$. In the decision rules (b&c), *solid / dash* lines indicate *tree path / causal relations*.

**Causal Explanations:** Our mimic tree $\phi$ captures the influence of latent features on action advantages $y$. Figure 5 (a) illustrates the top three layers of the mimic tree. We can interpret the influence of a split by visualizing the expected latent values after this split. For example, after implementing the split $f_1$, we obtain two child nodes ($cell_{2,1}$ and $cell_{2,2}$). We compute the expected latent values for the instances on these nodes ($\mathbb{E}_{n \in cell}(\boldsymbol{Z}_n)$) and visualize the $3^{rd}$ object with the decoder (since $Z_{3,1}$ captures the variation of the $3^{rd}$ object). These visualizations automatically capture the difference of object information after splitting. They show that the instances on $cell_{2,2}$ have shorter (vertical) distance between the bird and the upper pillar, and thus their advantages for the action "down" are larger. We verify this observation by sampling an instance from both child nodes respectively. This observation is consistent with game rules since performing the action "down" when the bird approaches the upper pillar can prevent potential crashes and thus has a larger advantage.

**(a)** *Causal Relation Extraction.* Since there is no (observed/unobserved) confounder between latent variables (section 4.1), our mimic tree can capture causal relations between splitting features and predictions. Similar to Causal Decision Trees (CDTs) [31], a tree split $f$ in our mimic tree represents a *context-specific causal relationship* between the splitting condition $f$ and the action advantage $\hat{y}_i^{tree}$.

The context is a series of value assignments of the latent features along the path from the root to the parent node of $f$. For example, the decision rule in Figure 5(b) states that having $Z_{3,4} \geq 0.71$ is casually related to an action advantage of 0.23 when the action is 'down' and $Z_{3,1} \geq 0.12$ (context).

**(b)** *Counterfactual Analysis.* Leveraging the generation ability of the IDOE decoder, our mimic tree enables counterfactual analysis to answer "what if we had" questions: we show the influence on tree prediction by intervening to set the value of $Z_{k,d}$ equal to some particular value, For example, in Figure 5(c), we compute $F_{tree}[f_0, f_1, \ldots, f_L, X', Y'_{\boldsymbol{\theta}}|\text{do}(Z_{3,1} = 0)]$. To achieve this, 1) we set $Z_{3,1}$ to 0 for all input latent vectors and get $\boldsymbol{z}'$. 2) The IDOE decoder computes $p_d(\boldsymbol{x}'|\boldsymbol{z}')$ and the DRL model predicts $Y'_{\boldsymbol{\theta}}$ with the generated observations $X'$. 3) The mimic tree follows previous splits to construct tree predictions (the splits on the intervened variables are removed). The difference of tree prediction before and after the intervention (0.23 versus 0.11) reveals the influence of $\text{do}(Z_{3,1} = 0)$.

**Comparison to other interpretations.** We compare other interpretable DRL models based on 1) Super-pixels [9] (Figure 5d) that highlight the pixels used as splitting features in a regression tree, 2) Saliency Map [3] (Figure 5e) which is generated by perturbing the pixels within a region and evaluating their impact on target outputs, and 3) Attention Mask [1] (Figure 5f) (from the convolutional attention network) that represents the importance of pixels on model outputs. These traditional models used the raw images as input during training. The learned interpretations visualize the pixels that are important for decisions. They generally agree that the distance between the bird and the pillar is most influential. This observation is consistent with rules extracted by our method (Figure 5a&b) since this distance determines how likely the bird can pass the pillars to win more rewards.

**Human Evaluation.** We evaluate the interpretability of the aforementioned methods with RL practitioners from four universities. We first introduce the saliency map, mimic trees based on super-pixels and latent variables, and then ask the participants to 1) describe the information captured by these methods and 2) rank the corresponding interpretations. To eliminate potential bias, participants are interviewed independently, and they are not told which methods are the baselines or the proposed model (check Section D in appendix for further details). We present a summary of the results by discussing the two aspects of interpretability regarding our method:

**(a)** *Interpretability of Latent Variables*. After observing the latent traversals, all (12/12) participants correctly recognized the physical meaning of the latent variables whereas 58%(7/12) and 33.3%(4/12) participants managed to recognize the features captured by saliency maps and super-pixels due to the inconsistency of local samples and the complexity of tree paths.

**(b)** *Interpretability of mimic trees*. 83% (10/12) participants preferred the mimic tree based on latent features since its tree path captures globally-consistent knowledge and its tree size is smaller than that of the super-pixel tree (62 versus 1007, check Table 1). The rest voted for the saliency map because they preferred straight-forward explanations.

### 6.3 Limitations

**Computational Complexity.** Since MCRTS conducts multiple simulations to explore and generate the global-optimal mimic tree, it generally consumes more computational resources than classic regression. We compare the computational complexity of our method and the baselines in the appendix. Although IDOE compresses high-dimensional inputs into latent vectors and we parallelize the tree search in MCRTS, empirically, it takes MCRTS a longer to determine a split.

**Guarantee for Interpretability.** It is generally hard to theoretically justify or numerically quantity the level of interpretability, so we utilize illustrative examples and human evaluation to empirically show the interpretability. Although previous works demonstrated interpretability of latent features [34, 39, 40], there is no guarantee that these features always have a clear meaning across all RL games.

## 7 Conclusion and Societal Impacts

This paper introduced a RAMi framework based on the IB principle, following which we 1) introduced an IDOE to learn an object representation for RL states and 2) proposed a MCRTS algorithm to find a mimic tree with promising fidelity and simplicity. Experiments demonstrated the leading mimic performance of our MCRTS+IDOE model. We illustrated our tree interpretations with causal relations and human evaluation. A potential *negative societal impact* of our work is that it encourages the government to endorse laws that regulate the level of transparency in AI systems. This may increase the difficulty of deploying advanced AI systems.

# References


[1] Wenjie Shi, Shiji Song, Zhuoyuan Wang, and Gao Huang. Self-supervised discovering of causal features: Towards interpretable reinforcement learning. *CoRR*, abs/2003.07069, 2020.

[2] Alexander Mott, Daniel Zoran, Mike Chrzanowski, Daan Wierstra, and Danilo Jimenez Rezende. Towards interpretable reinforcement learning using attention augmented agents. In *Advances in Neural Information Processing Systems 32: Annual Conference on Neural Information Processing Systems 2019, NeurIPS 2019, 8-14 December 2019, Vancouver, BC, Canada*, pages 12329–12338, 2019.

[3] Samuel Greydanus, Anurag Koul, Jonathan Dodge, and Alan Fern. Visualizing and understanding atari agents. In *Proceedings of the 35th International Conference on Machine Learning, ICML 2018, Stockholmsmässan, Stockholm, Sweden, July 10-15, 2018*, pages 1787–1796, 2018.

[4] Tom Zahavy, Nir Ben-Zrihem, and Shie Mannor. Graying the black box: Understanding dqns. In *Proceedings of the 33nd International Conference on Machine Learning, ICML 2016, New York City, NY, USA, June 19-24, 2016*, pages 1899–1908, 2016.

[5] Sarthak Jain and Byron C. Wallace. Attention is not explanation. In *Proceedings of the 2019 Conference of the North American Chapter of the Association for Computational Linguistics: Human Language Technologies, NAACL-HLT 2019, Minneapolis, MN, USA, June 2-7, 2019, Volume 1 (Long and Short Papers)*, pages 3543–3556, 2019.

[6] Sarah Wiegreffe and Yuval Pinter. Attention is not not explanation. In *Proceedings of the 2019 Conference on Empirical Methods in Natural Language Processing and the 9th International Joint Conference on Natural Language Processing, EMNLP-IJCNLP 2019, Hong Kong, China, November 3-7, 2019*, pages 11–20, 2019.

[7] David Alvarez-Melis and Tommi S. Jaakkola. On the robustness of interpretability methods. *CoRR*, abs/1806.08049, 2018.

[8] Jimmy Ba and Rich Caruana. Do deep nets really need to be deep? In *Advances in Neural Information Processing Systems 27: Annual Conference on Neural Information Processing Systems 2014, December 8-13 2014, Montreal, Quebec, Canada*, pages 2654–2662, 2014.

[9] Guiliang Liu, Oliver Schulte, Wang Zhu, and Qingcan Li. Toward interpretable deep reinforcement learning with linear model u-trees. In *Machine Learning and Knowledge Discovery in Databases - European Conference, ECML PKDD 2018, Dublin, Ireland, September 10-14, 2018, Proceedings, Part II*, pages 414–429, 2018.

[10] Xiangyu Sun, Jack Davis, Oliver Schulte, and Guiliang Liu. Cracking the black box: Distilling deep sports analytics. In *Proceedings of the 26th ACM SIGKDD International Conference on Knowledge Discovery and Data Mining, Virtual Conference, August 23-27, 2020*, 2020.

[11] Olcay Boz. Extracting decision trees from trained neural networks. In *Proceedings of the Eighth ACM SIGKDD International Conference on Knowledge Discovery and Data Mining, July 23-26, 2002, Edmonton, Alberta, Canada*, pages 456–461, 2002.

[12] Darren Dancey, Zuhair Bandar, and David McLean. Logistic model tree extraction from artificial neural networks. *IEEE Transactions on Systems, Man, and Cybernetics*, 37(4):794–802, 2007.

[13] Naftali Tishby, Fernando C Pereira, and William Bialek. The information bottleneck method. *arXiv preprint physics/0004057*, 2000.

[14] Daoming Lyu, Fangkai Yang, Bo Liu, and Steven Gustafson. SDRL: interpretable and data-efficient deep reinforcement learning leveraging symbolic planning. In *The Thirty-Third AAAI Conference on Artificial Intelligence, AAAI 2019, The Thirty-First Innovative Applications of Artificial Intelligence Conference, IAAI 2019, The Ninth AAAI Symposium on Educational Advances in Artificial Intelligence, EAAI 2019, Honolulu, Hawaii, USA, January 27 - February 1, 2019*, pages 2970–2977, 2019.

[15] Ujjwal Das Gupta, Erik Talvitie, and Michael Bowling. Policy tree: Adaptive representation for policy gradient. In *Proceedings of the Twenty-Ninth AAAI Conference on Artificial Intelligence, January 25-30, 2015, Austin, Texas, USA*, pages 2547–2553, 2015.

[16] Aaron M. Roth, Nicholay Topin, Pooyan Jamshidi, and Manuela Veloso. Conservative q-improvement: Reinforcement learning for an interpretable decision-tree policy. *CoRR*, abs/1907.01180, 2019.

[17] Zhengxian Lin, Kin-Ho Lam, and Alan Fern. Contrastive explanations for reinforcement learning via embedded self predictions. In *9th International Conference on Learning Representations, ICLR 2021, Conference Track Proceedings*, 2021.

[18] Anurag Koul, Alan Fern, and Sam Greydanus. Learning finite state representations of recurrent policy networks. In *7th International Conference on Learning Representations, ICLR 2019, New Orleans, LA, USA, May 6-9, 2019*. OpenReview.net, 2019.

[19] Alihan Hüyük, Daniel Jarrett, Cem Tekin, and Mihaela van der Schaar. Explaining by imitating: Understanding decisions by interpretable policy learning. In *9th International Conference on Learning Representations, ICLR 2021, Conference Track Proceedings*, 2021.

[20] Tom Bewley and Jonathan Lawry. Tripletree: A versatile interpretable representation of black box agents and their environments. *CoRR*, abs/2009.04743, 2020.

[21] Anthony Manchin, Ehsan Abbasnejad, and Anton van den Hengel. Reinforcement learning with attention that works: A self-supervised approach. In *Neural Information Processing - 26th International Conference, ICONIP 2019, Sydney, NSW, Australia, December 12-15, 2019, Proceedings, Part V*, pages 223–230, 2019.

[22] Mike Wu, Michael C. Hughes, Sonali Parbhoo, Maurizio Zazzi, Volker Roth, and Finale Doshi-Velez. Beyond sparsity: Tree regularization of deep models for interpretability. In *Proceedings of the Thirty-Second AAAI Conference on Artificial Intelligence, (AAAI-18), New Orleans, Louisiana, USA, February 2-7, 2018*, pages 1670–1678, 2018.

[23] Osbert Bastani, Yewen Pu, and Armando Solar-Lezama. Verifiable reinforcement learning via policy extraction. In Samy Bengio, Hanna M. Wallach, Hugo Larochelle, Kristen Grauman, Nicolò Cesa-Bianchi, and Roman Garnett, editors, *Advances in Neural Information Processing Systems 31: Annual Conference on Neural Information Processing Systems 2018, NeurIPS 2018, December 3-8, 2018, Montréal, Canada*, pages 2499–2509, 2018.

[24] Stéphane Ross, Geoffrey J. Gordon, and Drew Bagnell. A reduction of imitation learning and structured prediction to no-regret online learning. In Geoffrey J. Gordon, David B. Dunson, and Miroslav Dudík, editors, *Proceedings of the Fourteenth International Conference on Artificial Intelligence and Statistics, AISTATS 2011, Fort Lauderdale, USA, April 11-13, 2011*, volume 15 of *JMLR Proceedings*, pages 627–635.

[25] Vijay R. Konda and John N. Tsitsiklis. Actor-critic algorithms. In *Advances in Neural Information Processing Systems 12, [NIPS Conference, Denver, Colorado, USA, November 29 - December 4, 1999]*, pages 1008–1014, 1999.

[26] Martin A. Riedmiller. Neural fitted Q iteration - first experiences with a data efficient neural reinforcement learning method. In *Machine Learning: ECML 2005, 16th European Conference on Machine Learning, Porto, Portugal, October 3-7, 2005, Proceedings*, pages 317–328, 2005.

[27] Alexander A. Alemi, Ian Fischer, Joshua V. Dillon, and Kevin Murphy. Deep variational information bottleneck. In *5th International Conference on Learning Representations, ICLR 2017, Toulon, France, April 24-26, 2017, Conference Track Proceedings*, 2017.

[28] Diederik P. Kingma and Max Welling. Auto-encoding variational bayes. In *2nd International Conference on Learning Representations, ICLR 2014, Banff, AB, Canada, April 14-16, 2014, Conference Track Proceedings*, 2014.

[29] Mengyue Yang, Furui Liu, Zhitang Chen, Xinwei Shen, Jianye Hao, and Jun Wang. Causalvae: Structured causal disentanglement in variational autoencoder. *CoRR*, abs/2004.08697, 2020.

[30] Bernhard Schölkopf. Causality for machine learning. *CoRR*, abs/1911.10500, 2019.

[31] Jiuyong Li, Saisai Ma, Thuc Duy Le, Lin Liu, and Jixue Liu. Causal decision trees. *IEEE Transactions on Knowledge and Data Engineering*, 29(2):257–271, 2017.

[32] Francesco Locatello, Stefan Bauer, Mario Lucic, Gunnar Rätsch, Sylvain Gelly, Bernhard Schölkopf, and Olivier Bachem. Challenging common assumptions in the unsupervised learning of disentangled representations. In *Proceedings of the 36th International Conference on Machine Learning, ICML 2019, 9-15 June 2019, Long Beach, California, USA*, pages 4114–4124, 2019.

[33] Ilyes Khemakhem, Diederik P. Kingma, Ricardo Pio Monti, and Aapo Hyvärinen. Variational autoencoders and nonlinear ICA: A unifying framework. In *The 23rd International Conference on Artificial Intelligence and Statistics, AISTATS 2020, 26-28 August 2020, Online [Palermo, Sicily, Italy]*, pages 2207–2217, 2020.

[34] Christopher P. Burgess, Loïc Matthey, Nicholas Watters, Rishabh Kabra, Irina Higgins, Matthew Botvinick, and Alexander Lerchner. Monet: Unsupervised scene decomposition and representation. *CoRR*, abs/1901.11390, 2019.

[35] Olaf Ronneberger, Philipp Fischer, and Thomas Brox. U-net: Convolutional networks for biomedical image segmentation. In Nassir Navab, Joachim Hornegger, William M. Wells III, and Alejandro F. Frangi, editors, *Medical Image Computing and Computer-Assisted Intervention - MICCAI 2015 - 18th International Conference Munich, Germany, October 5 - 9, 2015, Proceedings, Part III*, volume 9351 of *Lecture Notes in Computer Science*, pages 234–241. Springer, 2015.

[36] Carlos Diuk, Andre Cohen, and Michael L. Littman. An object-oriented representation for efficient reinforcement learning. In William W. Cohen, Andrew McCallum, and Sam T. Roweis, editors, *Machine Learning, Proceedings of the Twenty-Fifth International Conference (ICML 2008), Helsinki, Finland, June 5-9, 2008*, volume 307 of *ACM International Conference Proceeding Series*, pages 240–247. ACM, 2008.

[37] Vikash Goel, Jameson Weng, and Pascal Poupart. Unsupervised video object segmentation for deep reinforcement learning. In Samy Bengio, Hanna M. Wallach, Hugo Larochelle, Kristen Grauman, Nicolò Cesa-Bianchi, and Roman Garnett, editors, *Advances in Neural Information Processing Systems 31: Annual Conference on Neural Information Processing Systems 2018, NeurIPS 2018, December 3-8, 2018, Montréal, Canada*, pages 5688–5699, 2018.

[38] Thomas N. Kipf, Elise van der Pol, and Max Welling. Contrastive learning of structured world models. In *8th International Conference on Learning Representations, ICLR 2020, Addis Ababa, Ethiopia, April 26-30, 2020*. OpenReview.net, 2020.

[39] Hyunjik Kim and Andriy Mnih. Disentangling by factorising. In *Proceedings of the 35th International Conference on Machine Learning, ICML 2018, Stockholmsmässan, Stockholm, Sweden, July 10-15, 2018*, pages 2654–2663, 2018.

[40] Irina Higgins, Loïc Matthey, Arka Pal, Christopher Burgess, Xavier Glorot, Matthew Botvinick, Shakir Mohamed, and Alexander Lerchner. beta-vae: Learning basic visual concepts with a constrained variational framework. In *5th International Conference on Learning Representations, ICLR 2017, Toulon, France, April 24-26, 2017, Conference Track Proceedings*, 2017.

[41] Abhishek Kumar, Prasanna Sattigeri, and Avinash Balakrishnan. Variational inference of disentangled latent concepts from unlabeled observations. In *6th International Conference on Learning Representations, ICLR 2018, Vancouver, BC, Canada, April 30 - May 3, 2018, Conference Track Proceedings*, 2018.

[42] J. Ross Quinlan and Ronald L. Rivest. Inferring decision trees using the minimum description length principle. *Information and Computation*, 80(3):227–248, 1989.

[43] Manish Mehta, Jorma Rissanen, and Rakesh Agrawal. Mdl-based decision tree pruning. In *Proceedings of the First International Conference on Knowledge Discovery and Data Mining (KDD-95), Montreal, Canada, August 20-21, 1995*, pages 216–221, 1995.

[44] Guillaume Chaslot, Mark H. M. Winands, and H. Jaap van den Herik. Parallel monte-carlo tree search. In *Computers and Games, 6th International Conference, CG 2008, Beijing, China, September 29 - October 1, 2008. Proceedings*, pages 60–71, 2008.

[45] Adrien Couëtoux, Jean-Baptiste Hoock, Nataliya Sokolovska, Olivier Teytaud, and Nicolas Bonnard. Continuous upper confidence trees. In *Learning and Intelligent Optimization - 5th International Conference, LION 5, Rome, Italy, January 17-21, 2011. Selected Papers*, pages 433–445, 2011.

[46] David Silver, Julian Schrittwieser, Karen Simonyan, Ioannis Antonoglou, Aja Huang, Arthur Guez, Thomas Hubert, Lucas Baker, Matthew Lai, Adrian Bolton, et al. Mastering the game of go without human knowledge. *Nature*, 550(7676):354–359, 2017.

[47] Norman Tasfi. Pygame learning environment. *GitHub repository*, 2016.

[48] Greg Brockman, Vicki Cheung, Ludwig Pettersson, Jonas Schneider, John Schulman, Jie Tang, and Wojciech Zaremba. Openai gym. *CoRR*, abs/1606.01540, 2016.

[49] Roman Timofeev. Classification and regression trees (cart) theory and applications. *Humboldt University, Berlin*, pages 1–40, 2004.

[50] John R Quinlan et al. Learning with continuous classes. In *5th Australian joint conference on artificial intelligence*, volume 92, pages 343–348. World Scientific, 1992.

# Checklist

1. For all authors...
   (a) Do the main claims made in the abstract and introduction accurately reflect the paper's contributions and scope? [Yes]
   (b) Did you describe the limitations of your work? [Yes] See Section 6.3.
   (c) Did you discuss any potential negative societal impacts of your work? [Yes] See Section 7. For a detailed discussion of ethics statement, please check section F in appendix.
   (d) Have you read the ethics review guidelines and ensured that your paper conforms to them? [Yes]
2. If you are including theoretical results...
   (a) Did you state the full set of assumptions of all theoretical results? [Yes] Please check the assumption of the IB objective in the Theorem 1 and the assumption of causal inference in section 4.1.
   (b) Did you include complete proofs of all theoretical results? [Yes] For the complete proof of Theorem 1, please check Section B in appendix.
3. If you ran experiments...
   (a) Did you include the code, data, and instructions needed to reproduce the main experimental results (either in the supplemental material or as a URL)? [Yes] Please check the attached code and Section A.2.2 in appendix for the data generation details.
   (b) Did you specify all the training details (e.g., data splits, hyperparameters, how they were chosen)? [Yes] Please check Section A.2.3 in appendix for the implementation details (including hyperparameters) of our model and all baseline models.
   (c) Did you report error bars (e.g., with respect to the random seed after running experiments multiple times)? [Yes] Please check Section C in appendix for the complete results (including mean and variance for 5 independent runs).
   (d) Did you include the total amount of compute and the type of resources used (e.g., type of GPUs, internal cluster, or cloud provider)? [Yes] Please check Section A.2.7 in appendix for the details of computing resource. Please check Section A.2.4 in appendix for the computational complexity of our method and other baselines.
4. If you are using existing assets (e.g., code, data, models) or curating/releasing new assets...

(a) If your work uses existing assets, did you cite the creators? [Yes] We cite the creators of Pygame learning environment and OpenAI gym toolkit in reference.

(b) Did you mention the license of the assets? [N/A] The assets creators posted the instructions about how to cite their works. We are not aware of mentioning the licenses.

(c) Did you include any new assets either in the supplemental material or as a URL? [N/A] We have not created new assets.

(d) Did you discuss whether and how consent was obtained from people whose data you're using/curating? [N/A] We have not used data from other people.

(e) Did you discuss whether the data you are using/curating contains personally identifiable information or offensive content? [N/A] Data from video game does not contain personal information.

5. If you used crowdsourcing or conducted research with human subjects...

(a) Did you include the full text of instructions given to participants and screenshots, if applicable? [Yes] Check Section D in appendix for the details of human evaluation.

(b) Did you describe any potential participant risks, with links to Institutional Review Board (IRB) approvals, if applicable? [N/A] Participants answered some questions regrading model evaluation. We did not collect any personal data.

(c) Did you include the estimated hourly wage paid to participants and the total amount spent on participant compensation? [N/A] Participants are volunteers. This message was properly delivered before any interview.